Silica-coating of nano-Y3Al5O12:Ce3+ synthesized by self-combustion

Robin Malo, Benoit Glorieux, Stéphane Mornet, Brice Mutelet, Laurence Vignau, Alain Garcia

Bull. Mater. Sci. (2019) 42:6
https://doi.org/10.1007/s12034-018-1701-4

Silica-coating of nano-$Y_3Al_5O_{12}:Ce^{3+}$ synthesized by self-combustion

ROBIN MALO[1,2], GLORIEUX BENOÎT[1,2,*], MORNET STÉPHANE[1,2], MUTELET BRICE[1,2], VIGNAU LAURENCE[3] and GARCIA ALAIN[1,2]

[1]ICMCB, UMR 5026, CNRS, 33600 Pessac, France
[2]ICMCB, UMR 5026, Université de Bordeaux, 33600 Pessac, France
[3]Bordeaux INP/ENSCBP, Laboratoire de l'Intégration du Matériau au Système, CNRS UMR5218, Université de Bordeaux, 33607 Pessac, France
*Author for correspondence (benoit.glorieux@icmcb.cnrs.fr)

MS received 11 December 2017; accepted 17 May 2018; published online 8 January 2019

Abstract. $Y_{2.91}Ce_{0.09}Al_5O_{12}$ is obtained by self-combustion, grinding and sol–gel coating. X-ray diffraction, transmission electron microscopy, photoluminescence and absorption measurements were used to identify the structural and optical properties of each step of the process. The process is composed of a combination of chemical and physico-chemical processes including combustion and thermal steps, followed by grinding, powder dispersion by acidic passivation, stabilization of particle dispersions with citrate ligands and embedding of yttrium aluminium garnet (YAG) particles into SiO_2 shells using a seeded growth process before drying. The initial state of the obtained powder is composed of 35 nm crystallites, sintered and agglomerated. The grinding step breaks the sintered bridge, while the passivation and citrate adsorption steps separate the particles by electrostatic repulsion before the silica coating. The optical characterizations are performed and compared separately for the powdered samples that represent the initial and final states of our process, and the dispersion sample represents the intermediate state of our process. The optical measurement revealed an important amount of optical defects at the surface of the particles, compared with micrometric commercial particles. The grinding, nitric acid and citrate steps remove some of these defects. The final state of the sample still possesses lower quantum efficiency than that of a micrometric sample, but the SiO_2 coating allows for a perfect separation of the particle, suitable for implementation in small devices.

Keywords. Self-combustion; YAG; core–shell; SiO_2 coating.

1. Introduction

Yttrium aluminium garnet (YAG) is one of the most widely used phosphors because of its ability to incorporate luminescent cations that induce the requested optical properties [1]. This material is also widely used due to its ease of synthesis [2], its excellent thermal and chemical stabilities [3] and its low number of optical defects, which allow for a high efficacy [4]. This compound, doped with neodymium (Nd-YAG; 355, 532 and 1064 nm) and erbium (Er-YAG; 2940 nm), is used as a ceramic in lasers to replace single-crystal YAG [5]. Other trivalent cations are also used as dopants, such as Yb, Ho, Cr, Tm, Tb, Dy and Sm, for some niche applications, cathode X-ray tubes, temperature sensors, non-linear optics and flash lamps [6,7]. YAG doped with cerium is a yellow phosphor used in phosphor-converted white light-emitting diodes (LEDs) [8], due to its ability to absorb blue light (450 nm) coming from the InGaN dye [9] and emit a broadband centred at 550 nm, inducing white light.

An additional strength of this compound is its ability to modulate specific properties of luminescent ions. The host structure (cubic, I_{a3d}) is modified by substituting yttrium and aluminium by other trivalent cations (Lu, Ga, etc.) and also by a pair of divalent and tetravalent cations (Mg–Si/Ge) [10]. These substitutions induce a modification to the cell parameters, the oxygen–cation distance, the angle of the distorted cubic site [11] and the crystal field surrounding the cation, all of these parameters having an influence on the optical properties.

YAG powder can be synthesized by various methods: solid-state reaction [12], co-precipitation [13], combustion [14], sol–gel process [15] and hydrothermics [16]. Pan *et al* [17] discussed the various optical properties of YAG:Ce^{3+} as a function of the synthesis method. In most cases, nano-sized compounds are of lower efficiency than micronic-sized compounds [18] due to the increase of the surface compared with the bulk. Moreover, the surface is the main source of optical defects due to poorly crystallized layers and the oxygen and hydroxyl bridge. According to our knowledge, only complicated and expensive experimental processes such as spray pyrolysis [19] allow for some phosphor-based nano-YAGs with a higher efficiency than micro-YAG to be obtained. Investigating nanoparticles may be worthwhile when scattering must be prevented or for integrating a device with a specific size smaller than 1 µm. In addition, in the cases of packaging nanoparticles in a small device, the

agglomeration process is a key issue. The goal is to avoid particle agglomeration in order to have a better dispersion of the particles. For this purpose, a well-known process is to add a silica shell surrounding the particle. Silica is of great interest in materials science due to its chemical inertness, optical transparency, thermal stability, dielectric properties, tunable porosity and ability to easily modify and formulate the surface in various media [20].

In this paper, we study the influence of a silica coating on the optical properties of Ce-YAG nanoparticles synthesized by a self-combustion technique. The effects of the various steps of the process are investigated by structural and optical measurements in order to understand the various mechanisms (physical and chemical) involved. Our process, starting and ending with powdered samples, implies intermediate stages with dispersion of the powder into liquid. Only powdered samples are characterized by electronic microscopy and X-ray diffraction (XRD). The optical characterizations are performed and compared separately for the powdered samples and the dispersion samples.

In the present study, a silica coating is used to promote the electrostatic colloidal stabilization of the YAG powders. The strategy uses a first step of surface leaching by acidic treatment in order to remove multivalent cations (Y^{3+} and Ce^{3+}) acting as ions determining potential (IDP) responsible for the decrease in the surface electrostatic potential preventing the particle's peptization [21]. The colloidal stabilization is then ensured by the adsorption of citrate ligands enabling the stabilization in alkaline medium. These dispersions can then be transferred to the sol–gel medium (alkaline hydro-alcoholic medium) for silica formation around the YAG particles by hydrolysis-condensation of tetraethoxysilane (TEOS). The isoelectric point value of pH 2–3 for the as-formed silica surface [22] makes these particles negatively charged for a large pH range of aqueous media.

2. Materials and method

2.1 *Materials*

Citric acid (99.5%) and TEOS (98+%) were purchased from Aldrich. Absolute ethanol (J.T. Baker) and ammonia (30%) were used as received. Water was deionized (resistivity higher than 18 MΩ). All other reagents were of analytical grade from Aldrich.

2.2 *Method*

$Y_{2.91}Ce_{0.09}Al_5O_{12}$ particles were synthesized by mixing $Y(NO_3)_3{\cdot}6H_2O$, $Ce(NO_3)_3{\cdot}6H_2O$ and $Al(NO_3)_3{\cdot}9H_2O$ with water in a stainless-steel beaker. Glycine (Alfa Aesar) was then added with a specific molar ratio glycine/nitrate of 0.55. After 30 min of stirring, the mixture was slowly heated at 80°C on a hot plate in order to evaporate water. The resulting viscous liquid was then heated at 250°C in order to achieve the self-combustion step. At this stage, the obtained product consists of voluminous dark ashes.

The obtained amorphous black powder was then treated at 900°C in a tubular furnace at a heating rate of 3°C min^{-1}. The sample was maintained at this temperature for 2 h in an air environment, and then 30 min in an argon environment followed by an additional 90 min under Ar/H_2 flow. This process removes the carbon residue and then crystallizes the YAG phase with a perfect reduction of cerium. The obtained powder is called heated-powder.

The powder is then grinded using ball milling for 1 h to break the particles prior to the core–shell process. The obtained powder is called grinded-powder.

YAG nanoparticles were coated by silica with a method previously reported [21,23,24]. The YAG particle surface was first treated with an acidic treatment under ultrasound (sonicator bath) for 15 min in 10 ml of 2 M HNO_3. After washing by centrifugation (3000g), the particle surfaces were citrated by adding 0.05 M solution of citric acid resulting in the flocculation of the particle dispersion. Citrated nanoparticles were washed again with ultra-pure water by centrifugation to remove excess citric acid. Peptization of the particles occurred by adding 200 µl of ammonia (30%) on the pellet before dilution in 100 ml of MilliQ water and 10 min of sonication. Then, the alkaline dispersion was poured into a volume of ethanol/water/ammonia solution 75/23.5/1.5%. The reaction volume was fixed at 800 ml. A volume of 1.2 ml of TEOS was found to give a silica coating thickness of 5 nm. The shell thickness was checked using transmission electron microscopy (TEM). A simple calculation provides a good starting TEOS volume. Considering the mean of Feret diameters measured by TEM, taking into account the number of particles N_p and assuming that particles are spherical, the starting TEOS volume was calculated using the formula $V_{TEOS} = 3.89 \times N_p(D^3 - d^3)$; V_{TEOS} is directly expressed in ml and D and d are the final and starting diameters expressed in cm. The 3.89 scaling factor was computed from the molecular weights of SiO_2 formula units and TEOS and the densities of silica and TEOS (2 and 0.934 g cm^{-3}, respectively). Typically, for 500 mg of grinded YAG dispersed particles, a volume of 1.2 ml of TEOS was added to give a silica thickness of approximately 5 nm. A last centrifugation yields the final product defined as the dried silica-coated powder.

In summary, the analysed samples are as follows:

- The heated powder from the thermally treated reagent after the self-combustion step.
- The grinded powder from the grinding process of the previous sample.
- The ultrasonic dispersion from the acidic treatment under ultrasound of the previous sample.
- The citrated particle dispersion from the critic acid treatment of the previous sample.
- The silica-coated particle dispersion from the TEOS treatment of the previous sample.

– Finally, the dried silica-coated powder from the centrifugation of the previous sample.

Due to the technical properties of the experimental characterization, only the powdered samples (heated, grinded and dried silica-coated) are analysed by XRD, TEM and photoluminescence and diffuse reflectance. The dispersed samples (ultrasonic, citrated and silica-coated) are characterized only by photoluminescence.

The ultrasonic dispersion can be assimilated to the grinded powder, since it is just the grinded powder dispersed in ethanol. The silica-coated particle dispersion can also be assimilated to the dried silica-coated powder.

3. Experimental

3.1 *X-ray diffraction*

The samples were characterized by powder XRD using a Bragg-Brentano Philips PW1820 diffractometer working with Cu Kα radiation and a backward monochromator. The patterns were analysed using Eva Bruker® software and compared with the PDF database using FindIt ICSD software. The cell parameters were calculated using the Rietveld refinement with FullProf software [25].

3.2 *Transmission electron microscopy*

TEM experiments were performed on JEOL 2200FS equipment with a Schottky field-emission gun operating at 200 kV. For the grinded powders, the TEM powdered samples were prepared by dispersing a few milligrams of powder in ethanol. One drop of the solution was deposited on a Formvar/carbon copper grid. For silica-coated YAG particles, a drop of the ethanolic dispersion was directly deposited on the grid after the coating step.

3.3 *Photoluminescence*

The luminescence properties were analysed using a SPEX FL212 spectrofluorometer. This equipment is composed of a 450 W xenon lamp, an excitation double monochromator, a sample holder, an emission double monochromator and a photomultiplier tube. The sample holder can be a black stainless-steel plate for powder samples or a quartz cuvette for liquid samples.

This equipment was also used to record the diffuse reflectance spectra of luminescent powder and to calculate the absorption. In this case, the emission and the excitation monochromators are in a synchronous mode to collect all of the diffuse reflections of the xenon lamp without catching any fluorescence photons. A black reference (B: black toner) and a white reference (W: magnesia MgO) were scanned under the same conditions, and the measurement for the sample (S) was corrected to obtain the desired data (R) following the relationship: $R = (S - B)/(W - B)$.

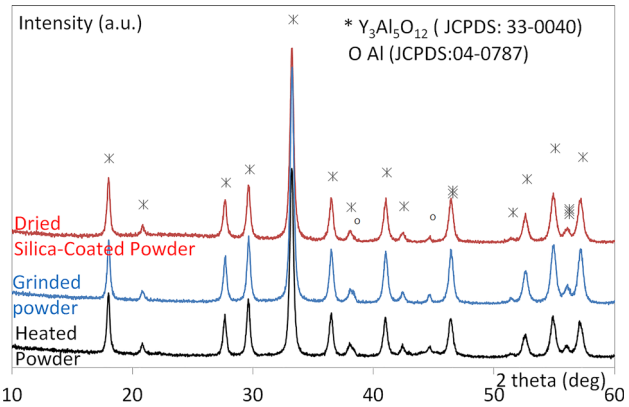

Figure 1. XRD patterns of nano-YAG: heated powder, grinder powder and dried silica-coated powder.

4. Results and discussion

4.1 *X-ray powder diffraction*

The heated powder, the grinded powder and the dried silica-coated powder were investigated by XRD. The results are shown in figure 1.

The peaks correspond perfectly to the YAG reference (JCPDS 33-0040). The aluminium peaks revealed at 38.3 and 44.6 nm correspond to the sample holder, which are not easy to eliminate due to the nanometric size of the particles and the penetration depth of the X-ray beam.

The cell parameter, identical for the three samples and calculated using Fullprof, $a = 12.0520(2)$ is in agreement with the usual cell parameters revealed in the literature. The crystallite size, calculated by the Scherrer formula based on the peaks width [26], is 35 nm. This value corresponds to an average coherent crystallized domain size. The non-evolution of the value indicated that the single-crystal part of the particle does not change during the grinding and the core–shell processes.

The increase in the background between 15 and 30° of the dried silica-coated powder is due to the diffusion band of the amorphous silica shell surrounding the particles.

4.2 *Morphology*

The same samples analysed by XRD, as well as heated, grinded and dried silica-coated powders were investigated by TEM. The results are shown in figure 2.

The micrograph of the heated powder reveals mainly agglomerated particles (figure 2a) chemically bound together. It was difficult to find isolated particles (figure 2c). These agglomerates are micrometric in size, which is definitely not suitable for small devices for specific applications. As seen

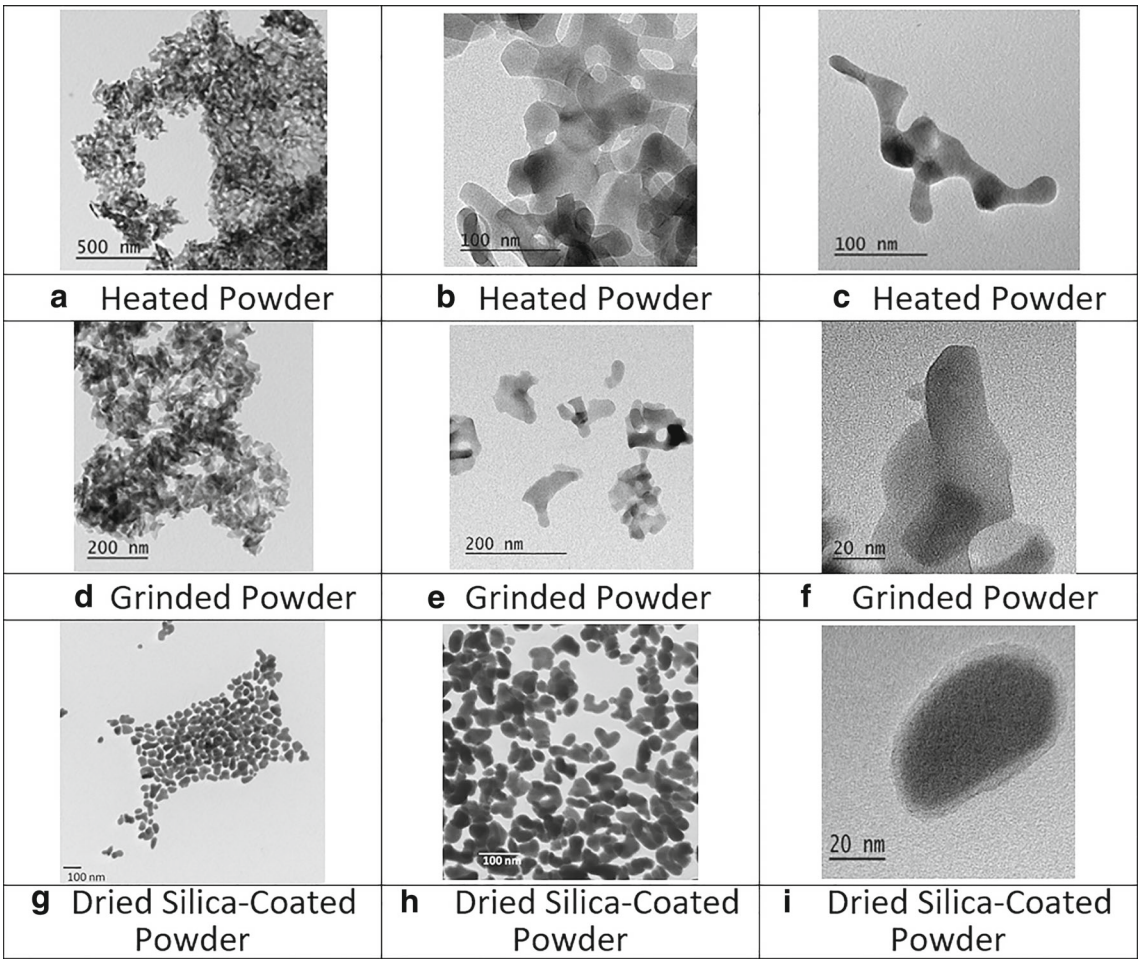

Figure 2. TEM micrographs of nano-YAG: heated powder, grinder powder and dried silica-coated powder.

in figure 2b and c, the particles are composed of various crystallites, sintered together with a YAG bridge. The size of the particles is approximately 40 nm, corresponding to the size calculated by X-rays.

By milling the powder, the agglomeration of particles is still revealed (figure 2d). However, looking more carefully (figure 2e and f), the edges of some particles appear sharp, revealing that the sintered bridge is broken by the grinding. The crystallite size is still approximately 40 nm.

The final product, the dried silica-coated powder, is a closed-packing of isolated particles resulting from the balance between the drying forces combined with the attractive van der Waals interactions and the repulsive electrostatic forces coming from the negatively charged silica surface (figure 2g and h). Isolated particles showed a uniform 5 nm silica shell surrounding the nanoparticles (figure 2i). The diffraction plans are also evidenced, revealing a well-crystallized state.

4.3 *Photoluminescence*

All samples were analysed by excitation and emission experiments. The emission measurements were performed by exciting at the maximum of the excitation band (453 nm). All the excitation measurements were performed by selecting the emission wavelength at the maximum of the emission band (551 nm). The powder sample measurements are shown in figure 3. The liquid sample measurements are shown in figure 4.

In all the cases, excitation spectra reveal two bands. The first one centred at 340 nm corresponds to the $^2F_{5/2}$-t_{2g} transition. There are in fact three split Gaussian contributions (in the energy range) in this band. The second band centred at 450 nm corresponds to the $^2F_{5/2}$-e_g transition [27]. There are in fact two split Gaussian contributions (in the energy range) in this band. This last band is used in LED devices to absorb the blue light coming from InGaN semiconductors [28].

In the emission spectra, the large bands, centred at 550 nm, are composed of two split Gaussian contributions due to the t_{2g}-$^2F_{5/2}$ and t_{2g}-$^2F_{7/2}$ transitions [27].

A commercial micrometric YAG was also analysed. The intensity measured for this last compound is approximately 40% higher than that of all the samples measured in the frame of this work. This finding means that as previously mentioned in the literature [29], nanometric compounds are less efficient

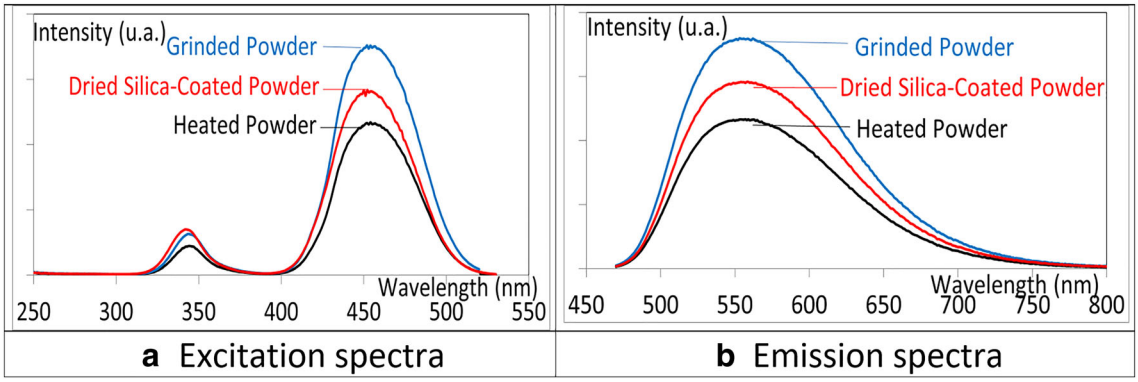

Figure 3. (**a**) Excitation and (**b**) emission of powder samples.

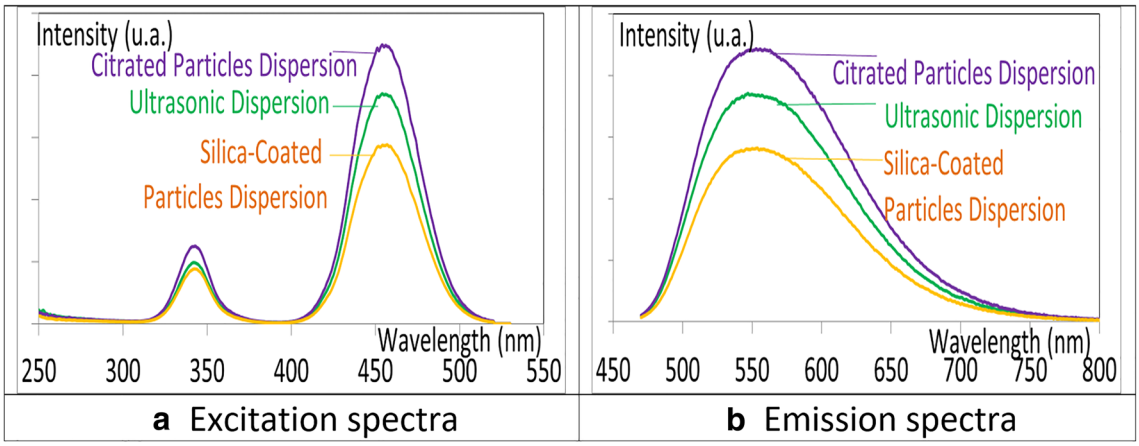

Figure 4. (**a**) Excitation and (**b**) emission of dispersed samples.

than micrometric ones due to the increase in surface defects in the nanometric materials.

For all the samples, there is neither modification of the shape nor the position of the maximum of each band, meaning that the crystallographic environment surrounding the cerium is not modified during all the processes.

However, there is a change in the intensity. For the powdered samples, the emission intensity is higher for the grinded powder than that for the heated powder, which means that the grinding process induces a modification to the particles. Indeed, during the grinding process, the particles are broken, inducing a change in their surface state. Knowing that the initial surface is a source of optical defects, the grinding process slightly decreases the part of the initial surface, lowering the amount of surface defects and increasing the efficiency.

The final compound, dried silica-coated powder, exhibits a similar intensity to the heated powder, meaning another surface modification appears during the shell coating.

For the liquid-dispersed samples, in the ultrasonic dispersion, the compounds can be assimilated to the grinded powder, since it is just the grinded powder that dispersed in ethanol. The dispersion was assisted by ultrasound and the measurements were performed. The goal was to avoid an agglomeration at the bottom part of the solution appearing during the measurement.

The citrated particle dispersion clearly exhibits a better efficiency compared with the ultrasonic dispersion sample. This is certainly due to the cleaning effect of the nitric acid, which removed some defects at the surface of the particles.

For the silica-coated particle dispersion sample, the intensity is lower. This might be due to the silanol (Si–OH) groups present at the particle surface, which can act as an electron trapper [30].

These experiments were reproduced many times. The various effects previously described occurred each time. However, the absolute value of the increase and decrease was not perfectly reproduced. A 20% variation was observed in the various identical experiments.

The last point observed in the photoluminescence measurement is the 340 *vs.* 450 nm intensity band ratio. Normalized excitation curves were calculated by setting the maximum of the 450 nm band to 1. The results are shown in figure 5. In this graph, an excitation of a commercial product is added in order to compare its properties with the ones obtained in this work.

A small shift in the $^2F_{5/2}$-t_{2g} transition (340 nm) and the $^2F_{5/2}$-e_g transition (450 nm) seems to be revealed between the powdered and the dispersion samples. This shift might be due to the crystallographic environment of the cerium but is more likely due to the packing effect of the samples.

Regarding the 450 nm band ($^2F_{5/2}$-e_g transition), there are three groups of data as a function of the bandwidth. The commercial product shows the broader band (full-width at half-maximum (FWHM): 77 nm), the powder samples have an average FWHM of 58 nm and the dispersed samples have an FWHM of 48 nm.

The dispersed particles exhibit the narrowest band shape. The grinded powder and the ultrasonic dispersion samples are basically the same samples: the first is a solid-state sample and the second is in a dispersed state. The same comparison can be performed for the silica-coated particle dispersion and the dried silica-coated powder. The difference in the band shape is due to the experimental process. In the solid state, the powders are compacted. The probability of excitation and emission light to hit a particle is important. The pathway of these beams is disturbed by multi-reflexion, while in the dispersed samples, particles are not as close as to each other, so the measured beam is less disturbed. In the commercial product, in addition to the packing effect, there is no selection of the particles. The crystallographic environment surrounding the cerium is not homogeneous in all the samples, inducing this broadening.

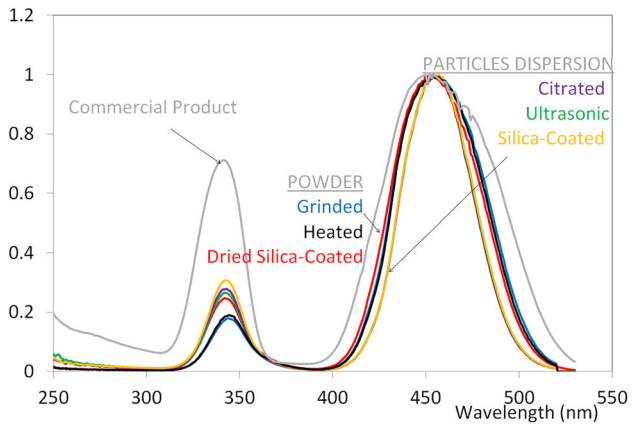

Figure 5. Normalized excitation spectra of all samples, including a commercial sample.

Regarding the 340 *vs.* 450 nm intensity band ratio, the commercial product is quite different from the nanoparticles. Among our samples, the silica-coated particle dispersion shows a higher ratio than the ultrasonic and citrated particle dispersions, which are almost equal and slightly higher than the dried silica-coated powder. The lowest ratio is for the heated and grinded powders. To analyse and understand this point, absorption measurement was performed on powder samples.

4.4 *Absorption*

The powder samples were analysed by diffuse reflection. These measurements reveal the phenomena responsible for a photonic transfer: radiative and non-radiative. Therefore, all the optical phenomena will be revealed: the excitation bands measured previously as well as optical defects. The results are shown in figure 6a and the normalized results in figure 6b.

The particle size is different for each sample, and the reference powders (magnesia and black toner) are of micronic size. This induces various pathways for the photons inside the samples. Therefore, the absolute measured values shown in figure 6 cannot be rationally analysed.

The points to be analysed are the positions, intensities and shapes of the absorption bands. The position of the 450 nm band did not shift, revealing again that there is no crystallographic modification in the environment of the cerium. The relative intensities of the absorption band centred at 450 nm are of the same order of magnitude as the excitation intensity shown in figure 3a, due to the grinding effect on the surface of the particles and the surface modification by the silica coating.

The most interesting point is an additional band below 400 nm, increasing in the UV range and overlapping the $^2F_{5/2}$-t_{2g}

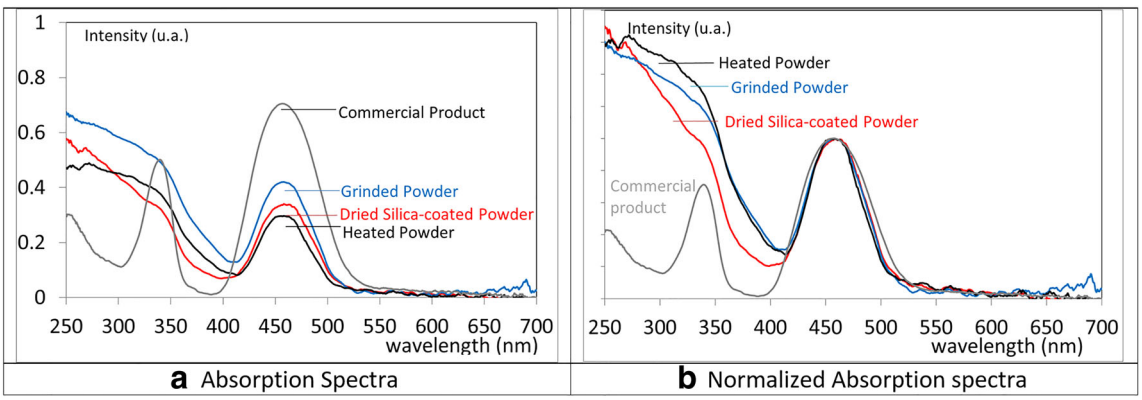

Figure 6. (**a**) Absorption and (**b**) normalized absorption spectra of powder particles.

transition (centred at 340 nm). This band is less intense for the commercial product. The large band below 400 nm corresponds to absorption giving rise to a non-radiative transfer, due to defects. It means that there are fewer defects in the commercial product than in the nanoparticles, which is expected since there is more surface in the nanoparticles than in the micronic ones. In fact, we analysed various commercial products from various companies. In addition, the measurements corresponding to this non-radiative band are different as a function of the retailer but also as a function of the synthesis batch coming from the same retailer.

Regarding the nanoparticles, the intensity of this last absorption band below 400 nm is inversely proportional to the intensity of the $^2F_{5/2}$-t_{2g} transition shown in figure 5. Therefore, below 400 nm, there is clearly a competitive phenomenon between the absorption of the $^2F_{5/2}$-t_{2g} transition of Ce^{3+} and the absorption of defects. The normalized absorption spectra (figure 6b) reveal that there are more defects in the heated powder than in the grinded powder and more in the grinded powder than in the dried silica-coated powder. This finding may explain the 340 *vs.* 450 nm intensity band ratio described previously (figure 3a). It means that in the initial synthesis, there is a great number of defects due to the important surface. The grinding process breaks some sintered bridges and creates new and clean surfaces that relatively decrease the amount of initial surface. Finally, the silica coating of the YAG particles removes some of these defects, by the acidic leaching influence and by the SiO_2 coating.

None of these defects seems to have an influence on the emission properties after the 450 nm excitation (figure 3b), since this non-radiative band disappears at 400 nm.

5. Conclusion

In this paper, the synthesis of $Y_{2.91}Ce_{0.09}Al_5O_{12}$ nanoparticles by self-combustion and the SiO_2 core–shell process have been clearly described. The XRD and the microscopy analyses confirm that the average coherent crystallized domain size of 35 nm is not modified during the process, revealing that the crystallographic structure of the particles is unchanged. This is confirmed by the luminescence study.

The various steps of the process (grinding, dispersion, acid leaching and citrate adsorption, silica coating and drying) induce many modifications to the surface state of the particles. The photoluminescence and the absorption measurements accurately describe this effect. While the most efficient sample in terms of optical efficiency is the grinded powder, the agglomerated state of the powder is a real limitation for their implementation in small devices. To this end, the covering of the YAG particles by an ultrathin silica layer, which efficiently separates and stabilizes colloidal dispersions, appears to be a promising route for such an objective.

References

[1] Emsley J (ed) 2000 *The shocking history of phosphorus* (UK: Macmillan)
[2] Bhattacharyya S and Ghatak S 2007 *Trans. Indian Ceram. Soc*. **66** 77
[3] Ye S, Xiao F, Pan Y X, Ma Y Y and Zhang Q Y 2010 *Mater. Sci. Eng. R* **71** 1
[4] Wu J L, Gundiah G and Cheetam A K 2007 *Chem. Phys. Lett*. **441** 250
[5] Kim J W, Shen D Y, Sahu J K and Clarkson A W 2009 *IEEE J. Sel. Top. Quantum Electron*. **15** 361
[6] Saiki T, Imasaki K, Motokoshi S, Yamanaka C, Fujita H, Nakatsuka M *et al* 2006 *Opt. Commun*. **268** 155
[7] Geusic J E, Marcos H M and Van Uitert L G 1964 *Appl. Phys. Lett*. **4** 182
[8] Mueller-Mach R, Mueller G O and Krames M 2004 *Proc. Third SPIE Int. Conf. Solid State Light*. **5187** 115
[9] Blasse G and Bril A 1967 *Appl. Phys. Lett*. **11** 53
[10] Dorenbos P 2013 *J. Lumin*. **134** 310
[11] Kanke Y and Navrotsky A 1998 *J. Solid. State Chem*. **141** 424
[12] Kupp E R, Kochawattana S, Lee S H, Misture S and Messing G L 2014 *J. Mater. Res*. **29** 2303
[13] Marlot C, Barraud E, Le Gallet S, Eichhorn M and Bernard F 2012 *J. Solid. State Chem*. **191** 114
[14] He G, Liu G, Yang Z, Guo S and Li J 2014 *Ceram. Int. B* **40** 15265
[15] Boukerika A, Guerbous L and Brihi N 2014 *J. Alloy. Compd*. **614** 383
[16] Yang H, Yuan L, Zhu G, Yu A and Xu H 2009 *Mater. Lett*. **63** 2271
[17] Yuexiao P, Mingmei W and Qiang S 2004 *Mater. Sci. Eng. B* **106** 251
[18] Yan B and Su X Q 2004 *Mater. Sci. Eng. B* **116** 196
[19] Chung W, Yu H J, Park S H, Chun B-H and Kim S H 2011 *Mater. Chem. Phys.* **126** 162
[20] Wang D, Caruso Rachel A and Caruso F 2001 *Chem. Mater*. **13** 364
[21] Mornet S, Elissalde C and Hornebecq V 2005 *Chem. Mater*. **17** 4530
[22] Iler Ralph K (ed) 1979 *The chemistry of silica* (USA: Wiley) 98
[23] Mornet S, Elissalde C and Bidault O 2007 *Chem. Mater*. **19** 987
[24] Kaman O, Pollert E, Veverka P, Hadova E, Knivek K, Marysko M *et al* 2009 *Nanotechnology* **20** 275610
[25] Roisnel T and Rodriguez-Carvajal J 2000 *Mater. Sci. Forum, Proc. 7th European Powder Diffr. Conf. (EPDIC 7)* **278-3** 118
[26] Patterson A L 1939 *Phys. Rev*. **56** 978
[27] Robbins D J 1979 *J. Electrochem. Soc*. **126** 1550
[28] Keating S, Urquhart M G, McLaughlin D V P and Pearce J M 2011 *Cryst. Growth Des*. **11** 565
[29] Li J, Zhao J, Zhou H, Liang J, Liu X and Xu B 2011 *Spectrochim. Acta A* **78** 1310
[30] Chua L L, Zaumseil J, Chang J F, Ou E C W, Ho P K H, Sirringhaus H *et al* 2005 *Nature* **434** 194